Model for reflectance anisotropy spectra of molecular layered systems

Bernardo S. Mendoza and R. A. Vázquez-Nava
Department of Photonics,Centro de Investigaciones en Optica, León, Guanajuato, México
(Received 30 December 2004; revised manuscript received 15 March 2005; published 5 July 2005)

We present a theoretical study based on the local field interaction for the reflectance anisotropy spectra of organic molecular layers. Each layer is formed by an ordered two-dimensional array of polarizable organic molecules that respond to the local electric field like point-like harmonic oscillators. We concentrate on the morphological characteristics of the layers and its effect on the spectra, showing that the reorientation of the molecules from layer to layer, as the system is assembled, gives rise to a line shape of the spectra that goes from peak-like to derivative-like. Our spectra shows good qualitative agreement with experimental results of a layered system of metalloporphyrin octaesters molecules deposited onto an isotropic gold substrate by the Langmuir-Schaefer technique.

DOI: 10.1103/PhysRevB.72.035411 PACS number(s): 78.40.Me, 78.66.−w, 78.20.−e

I. INTRODUCTION

Optical spectroscopic techniques are increasingly used nowadays to investigate surfaces and interfaces. Both linear and nonlinear optical probes are employed to investigate very different physical aspects of surfaces with great success.[1,2] In particular, reflectance anisotropy spectroscopy (RAS) has received growing attention from the experimental and theoretical sides, since it is one of the few optical techniques that probes the surface and interface structure of cubic materials directly. It measures the difference between the normal-incidence optical reflectance of light polarized along the two principal axes in the surface plane as a function of the photon energy. RAS data are typically obtained in the visible-ultraviolet spectral range, thus providing information about electronic structure modifications due to the creation of the surface, reconstructions, adsorbates, surface electric fields, etc.[1,2]

In recent years, considerable interest in the study of molecular materials has been aroused due to their large potential impact on nanotechnology. The characterization of electronic states in the fabricated molecular structures is essential. Recently, RAS has been applied to organic layers, showing that the spectra are reliably connected to the electronic properties of the molecule and to the morphological characteristics of the layer.[3–5] Optical techniques have been demonstrated to be particularly useful to characterize the arrangements of metalloporphyrin octaesters molecules, which we simply call porphyrins, in Langmuir-Schaefer films. In particular, the use of polarized light offers the possibility of studying systems that exhibit anisotropies due to electronic or morphological characteristics of the organic layer grown onto an isotropic substrate,[6,7] in analogy to what has been done in the case of semiconductor growth by means of RAS.[1,2]

In this article, we use a polarizable dipole model,[8] based on the local electric field interaction, to study the RAS effects due to the arrangement of organic molecular layered systems. The molecular layers are deposited onto an isotropic substrate by the Langmuir-Schaefer technique, which ensures a highly ordered deposition. We show how the line shape of the RAS spectra changes as a function of the two-dimensional (2D) arrangement of the molecules on the same plane. Recently, in Ref. 4, RAS was measured as a function of the number of layers for a porphyrin system, and an abrupt change in the RAS line shape at 8–10 monolayer coverage was found: the line shape, which at lower coverage is essentially proportional to the Soret band absorption and thus peak-like, becomes derivative-like. It is argued that this change may be due to a structural change in the porphyrin orientation. With the model presented here, we find that this change could be readily related to morphological changes on the layers of the films.

The article is organized as follows. In Sec. II we describe the polarizable dipole model, show how the geometrical arrangement of the molecules is taken into account, and explain the procedure to obtain RAS. In Sec. III we present and discuss the theoretical results for different geometries, and in Sec. IV we compared our results with those of the experiment. Finally, in Sec. V we give our conclusions.

II. THEORY

We study the optical response of a system composed of L molecular layers sitting on top of an optically isotropic substrate (see Fig. 1). Each layer consists of N identical nonoverlapping molecules that we take as polarizable entities ordered in a 2D Bravais lattice (see Fig. 2). In a given plane,

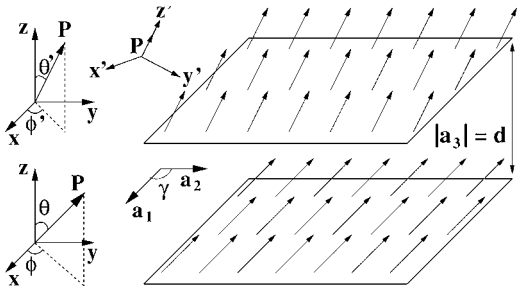

FIG. 1. Sketch of a system composed of molecular layers. The arrows represent the molecules (polarizable entities) and the planes with arrows represent a layer of molecules, with equal θ and ϕ. The molecules on the upper plane show a change in the tilt and twist angle with respect to those of the lower plane. $x(x')$, $y(y')$, and $z(z')$ are the coordinates of the system (molecule), and $\boldsymbol{a}_1$, $\boldsymbol{a}_2$, and $\boldsymbol{a}_3$ represent the primitive lattice vectors.

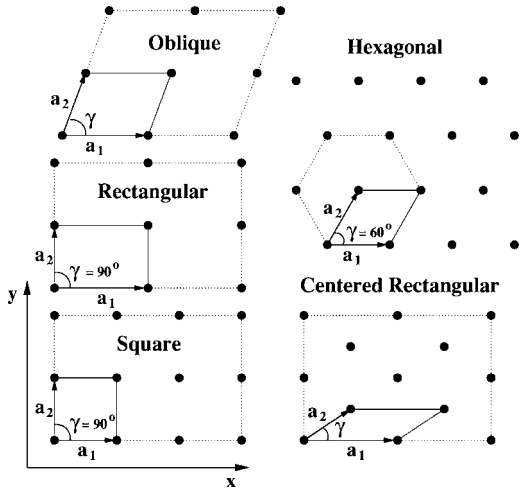

FIG. 2. The five 2D Bravais lattices, with the choice of the primitive unitary cell for each lattice (solid lines). x, y are the system's coordinates, $\boldsymbol{a}_1$, $\boldsymbol{a}_2$ represent the primitive lattice vectors and γ is the angle between them.

the polarizable entities have the same dipole orientation, characterized by the polar angle θ and azimuthal angle ϕ with respect to the sample coordinate system (see Fig. 1). However, in general, each plane has its own θ and ϕ. In addition, the planes are evenly spaced by a distance d, and we take, without loss of generality, that the first plane is at a distance $d/2$ from the substrate.

We assume that each molecule responds to the incident electric field like a harmonic oscillator, and take the long-wavelength limit to represent the optical activity of the molecules by point dipoles located at the center of mass of the molecule. We assume that the dipole polarizability, $\alpha'_{ij}(\omega)$, is diagonal in its own coordinate system (x',y',z'), and is given by

$$\alpha'_{ij}(\omega) = \begin{pmatrix} 0 & 0 & 0 \\ 0 & 0 & 0 \\ 0 & 0 & \alpha_0(\omega) \end{pmatrix}, \tag{1}$$

implying that the molecule only polarizes along its principal axis taken as z', where the indices i,j denote Cartesian coordinates. For a harmonic oscillator we can write

$$\alpha_0(\omega) = \frac{e^2 f_0/m\omega_0^2}{1-(\omega/\omega_0)^2 - i(\omega/\omega_0)[1/(\omega_0\tau)]}, \tag{2}$$

where ω_0 is the resonant frequency, τ is a damping parameter related to the width of the resonance, f_0 is the oscillator strength, and m and e the electron's mass and charge, respectively.

In general, the induced dipole moment of molecule n in plane ℓ, $p_i(n,\ell,\omega)$, is given by

$$p_i(n,\ell,\omega) = \alpha_{ij}(n,\ell,\omega)\mathcal{E}_j(n,\ell,\omega), \tag{3}$$

where $\boldsymbol{\mathcal{E}}$ is the local electric field of frequency ω, and $\boldsymbol{\alpha}$ is the polarizability tensor expressed in the sample coordinate system, given through

$$\alpha_{ij}(n,\ell,\omega) = R_{ik}(n,\ell)R_{jl}(n,\ell)\alpha'_{kl}(n,\ell,\omega), \tag{4}$$

where the sum over repeated indices is assumed. The rotation matrix R_{ij} is obtained from the multiplication of the following two matrices:

$$R^z(n,\ell) = \begin{pmatrix} \cos\phi_{n\ell} & -\sin\phi_{n\ell} & 0 \\ \sin\phi_{n\ell} & \cos\phi_{n\ell} & 0 \\ 0 & 0 & 1 \end{pmatrix}, \tag{5}$$

and

$$R^{y'}(n,\ell) = \begin{pmatrix} \cos\theta_{n\ell} & 0 & -\sin\theta_{n\ell} \\ 0 & 1 & 0 \\ \sin\theta_{n\ell} & 0 & \cos\theta_{n\ell} \end{pmatrix}, \tag{6}$$

where R^z ($R^{y'}$) is a rotation through an angle ϕ_ℓ (θ_ℓ) around the z (y') axis, thus $R_{ij}=R^z_{ik}R^{y'}_{kj}$ is the rotation that takes us from the molecule's coordinates to the sample coordinate system. The plane index ℓ implies that molecules sited on different planes can have different orientation; i.e., $\theta_\ell \neq \theta_{\ell'}$ and/or $\phi_\ell \neq \phi_{\ell'}$.

The local field, in the long-wavelength approximation, is given by

$$\mathcal{E}_i(n,\ell,\omega) = E_i^{ext}(\omega) + {\sum_{n'\ell'}}' M_{ij}(n,\ell;n',\ell')p_j(n',\ell',\omega), \tag{7}$$

where the first term is the position-independent external field, the second term is the dipolar field produced by all other dipoles, and the prime in the sum means that $n=n'$ and $\ell=\ell'$, being the self-interaction, is omitted from the sum. The tensor

$$M_{ij}(n,\ell;n'\ell') = \nabla_i\nabla_j \left.\frac{1}{|\vec{r}-\vec{r}_{n'\ell'}|}\right|_{\vec{r}=\vec{r}_{n\ell}}, \tag{8}$$

yields the dipolar interaction between the dipoles $n\ell$ and $n'\ell'$. We assume that all the molecules of the system are identical, and that for a given plane they have the same orientation θ and ϕ. Then, the summation over n' in Eq. (7) can be carried out assuming an infinite number of dipoles per plane and using standard plane-wise schemes that produce intra- and interplane terms.[9] Therefore, the local field can be written as

$$\begin{aligned}\mathcal{E}_j(\ell,\omega) = E_j(\omega) + \sum_{\ell'=1}^{L} \Big(& [T_{jk}(|\mathbf{a}_1|,|\mathbf{a}_2|,\gamma)\delta_{\ell\ell'} \\ & + \mathcal{T}_{jk}(|\mathbf{a}_1|,|\mathbf{a}_2|,\gamma,|z_\ell - z_{\ell'}|)(1-\delta_{\ell\ell'})]\delta_{kl} \\ & + \frac{\epsilon_2(\omega)-\epsilon_1(\omega)}{\epsilon_2(\omega)+\epsilon_1(\omega)}\mathcal{T}_{jk}(|\mathbf{a}_1|,|\mathbf{a}_2|,\gamma,|z_\ell + z_{\ell'}|)S_{kl}\Big) \\ & \times p_l(\ell',\omega),\end{aligned} \tag{9}$$

where ℓ, $\ell'=1,2,\ldots,L$, with L the total number of planes. As discussed above, $T_{ij}(|\boldsymbol{a}_1|,|\boldsymbol{a}_2|,\gamma)=\Sigma_{n'}^{\infty}M_{ij}(n,\ell;n',\ell)$, is recognized as the intraplane dipolar interaction tensor that

gives the local field contribution of the dipoles on the same plane ($\ell=\ell'$), and $\mathcal{T}_{ij}(|\boldsymbol{a}_1|,|\boldsymbol{a}_2|,\gamma,z)=\Sigma_{n'}^{\infty}M_{ij}(n,\ell;n',\ell')$ as the interplane dipolar interaction tensor that gives the local field contribution of the dipoles in plane ℓ with those of plane $\ell'\neq\ell$, where z is the interplane separation and z_ℓ is the vertical position of the ℓth plane. With these tensors, the third term in Eq. (9) gives the contribution of the planes on top of the substrate, whereas the fourth term gives the contribution coming from the images located inside the substrate, as can be recognized by the screening factor given by the dielectric functions $\epsilon_1(\omega)$ of the system, and $\epsilon_2(\omega)$ for the substrate, and $S_{ij}=\mathrm{diag}(-1,-1,1)$ gives the correct orientation of the image dipoles. As we see, the notation has simplified, since now, the induced dipole is the same for each plane ℓ, thus n has dropped from the aforementioned sums that define both $\mathbf{T}$ and $\boldsymbol{\mathcal{T}}$. However, their arguments $|\boldsymbol{a}_1|$, $|\boldsymbol{a}_2|$, γ, and z, denote their dependence on these geometrically related variables, that are inherited by the local field and the induced polarization, but not shown explicitly in neither $\boldsymbol{E}$ nor $\boldsymbol{p}$. We can then rewrite Eq. (3) as

$$p_i(\ell,\omega)=\alpha_{ij}(\ell,\omega)\mathcal{E}_j(\ell,\omega). \tag{10}$$

Since $\boldsymbol{\mathcal{E}}(\ell,\omega)$, also depends on $\boldsymbol{p}(\ell,\omega)$, Eq. (10) defines a system of equations that has to be solved for $\boldsymbol{p}(\ell,\omega)$.

The solution of Eq. (10) is straightforward, and once we have solved for $\boldsymbol{p}(\ell,\omega)$, we follow Ref. 10, to calculate the RAS signal of the system ($\mathcal{R}$) as the normalized change in reflectance through,

$$\mathcal{R}\equiv 8\pi\left(\frac{d}{\lambda}\right)\frac{1}{p_o}\sum_{\ell=1}^{L}[\mathrm{Im}(p_x(\ell,\omega))-\mathrm{Im}(p_y(\ell,\omega))], \tag{11}$$

with λ the wavelength of the incident light, d the aforementioned interplane distance, and p_o a normalization factor with the units of dipole moment used to set the scale of $\mathcal{R}$. Notice that $\mathcal{R}$ depends on the 2D geometry of the array of dipoles through the dipolar tensors $\mathbf{T}$ and $\boldsymbol{\mathcal{T}}$, and also depends on the orientation angles θ and ϕ of the molecules through the polarizability $\boldsymbol{\alpha}$, as can be easily seen from above equations.

It is instructive to solve Eq. (10) for only one plane, since the dependence of the polarization on the orientation angles can be easily understood. This is equivalent to neglect the interplane interaction. We get,

$$[p_x(\omega),p_y(\omega)]=\frac{e^2f_0}{m\omega_0^2}\sin^2\theta(\cos^2\phi E_x,\sin^2\phi E_y)\mathcal{D}, \tag{12}$$

where

$$\mathcal{D}^{-1}=1-\left(\frac{\omega}{\omega_0}\right)^2-i\left(\frac{\omega}{\omega_0}\right)\left(\frac{1}{\omega_0\tau}\right)-\frac{e^2f_0}{m\omega_0^2}\big[T_{zz}\cos^2\theta+(T_{xx}\cos^2\phi+T_{yy}\sin^2\phi)\sin^2\theta\big], \tag{13}$$

and p_z is not needed in Eq. (11). From Eq. (12) we see that in general, the magnitude and the resonant frequency of the induced dipole moment, given through the poles of $\mathcal{D}$, depend on the angles θ and ϕ, as well as $\boldsymbol{T}$, which has the implicit dependence on the geometry of the Bravais lattice. The subtle dependence on f_0 is fixed as we take it as a constant. Note that $p_x=p_y=0$ for $\theta=0$, since the dipoles would point along z only, and thus $\mathcal{R}=0$. From Eq. (13), we see that the resonance of the isolated dipole, centered at ω_0, is shifted by the interaction with the neighboring dipoles, on the same plane, through the local field. There are some special cases, for example, when the lattice is cubic $T_{xx}=T_{yy}=T_{zz}$ and the dependence on both angles cancels in $\mathcal{D}$, then the variation of θ or ϕ will produce only a change on the magnitude of the induce dipole. In the case of a square or hexagonal 2D lattice, $T_{xx}=T_{yy}$, then $\mathcal{D}$ will depend only on θ. Finally we notice that $p_x(\ell)\neq p_y(\ell)$ for a finite $\mathcal{R}$, and thus the geometry of the lattice and the orientation of the molecule should be such that the x and y components of the induced dipole moment are different. For all the lattices, $\mathcal{R}(\phi=45°)=0$.

III. RESULTS

In this section, we study how the RAS spectra changes as a function of the Bravais lattice and the polar and azimuthal orientation of the dipoles. To chose some of the parameters involved in the calculation, we take the experimentally studied porphyrin layered system deposited onto a polished gold substrate of Ref. 4. To compare on equal grounds the RAS spectra of the different geometries, we take the 2D unit cell area $A=|\boldsymbol{a}_1\times\boldsymbol{a}_2|$ as a constant. For instance, we use $A=55$ Å^2, which is equal to the area per molecule corresponding to the surface pressure of 30 mN/m used at deposition time in the samples of Ref. 4. We also take the separation between each molecular plane $d=43$ Å, which corresponds to the thickness measured by atomic force microscopy.[4] Therefore, the density of molecules by plane will be also the same for all our examples. From $A=55$ Å^2, we can estimate that $|\boldsymbol{a}_1|$ and $|\boldsymbol{a}_2|$ are of the order of $\sqrt{55}$ Å which is smaller than the interplane distance d. In addition, the porphyrin shows a well-defined absorption peak at $\lambda_0=2\pi c/\omega_0=387$ nm and width $1/(\omega_0\tau)=0.25$, which is known as the Soret band, and it is around this band where the RAS experiments are performed.[4] For the parameters chosen for $|\boldsymbol{a}_1|$ and $|\boldsymbol{a}_2|$, $f_0\sim 20$ gives a resonance around $\lambda_0=387$ nm. Finally the value of p_o is chosen such that it gives a similar amplitude of the calculated and the experimentally measured $\mathcal{R}$,[11] and take $\epsilon_1=2.5$ for the porphyrins and $\epsilon_2(\omega)$ for gold from Ref. 12.

To understand how the different parameters change $\mathcal{R}$, we fix the lattice and begin with the simplest of the Bravais lattices, the square lattice. Besides the number of planes, once the lattice is chosen, there is only the angles θ and ϕ left as parameters. We first vary θ for a given $\phi\neq 45°$, since for any lattice, $\mathcal{R}(\phi=45°)=0$. In Fig. 3 we show $\mathcal{R}$ for $L=1$ as a function of λ for different values of θ and fixed $\phi=42°$. We see that as θ increases the peak-like structure shifts to longer wavelengths, while its intensity and broadening increase. Similar behavior is found for the hexagonal lattice. The θ-dependence on the numerator of Eq. (12) changes the peak magnitude, while the θ-dependence of $\mathcal{D}$ [Eq. (13)] shifts the resonant frequency through the local field. Since θ controls the position of the resonance, we take $\theta\sim 55°$ to

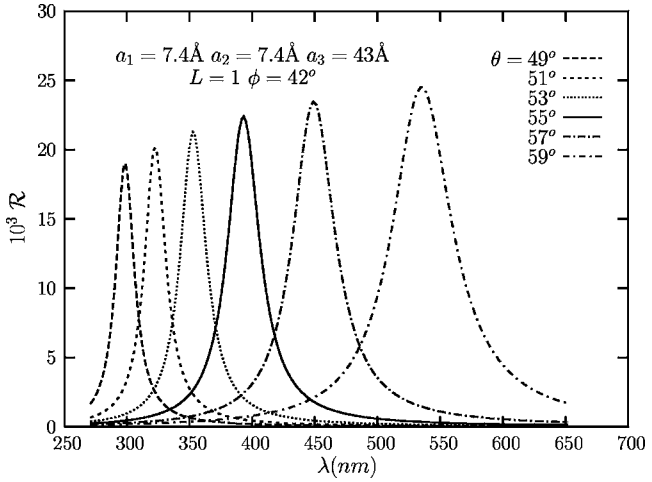

FIG. 3. $\mathcal{R}$ vs λ for a square 2D lattice with $L=1$ and $\phi=42°$, for several values of θ.

coincide with the experimental RAS result (see Fig. [9] below), which gives a redshifted Soret band for $\lambda \sim 395$ nm.[4]

Now we analyze how the spectrum changes as a function of ϕ. In Fig. 4 we show $\mathcal{R}$ for the same square lattice of the previous figure, but for several values of ϕ and a fixed $\theta = 55°$. The amplitude of $\mathcal{R}$ changes and its sign is reversed when ϕ crosses 45°. The same behavior is seen for the hexagonal geometry and is explained by the ϕ-dependence of Eqs. (12) and (13). For the square and hexagonal lattices the relation $T_{xx}=T_{yy}$ is satisfied, so that the ϕ-dependence of $\mathcal{D}$ drops out and only the simple ϕ-dependence of Eq. (12) remains, which only changes the projection of each component of $\boldsymbol{p}$ and thus only changes the magnitude of $\mathcal{R}$. For ϕ such that $p_x > p_y$, $\mathcal{R}$ is positive, otherwise is negative.

For the rectangular lattice $\mathcal{R}$ presents a red- or blueshift in addition to the change of the peak magnitude and sign. The direction of such a shift depends on which axis, x or y, is parallel to the largest side of the rectangle, as is shown in Fig. 5. For $a_1 > a_2$ ($a_1 < a_2$) the peak is redshifted (blue-

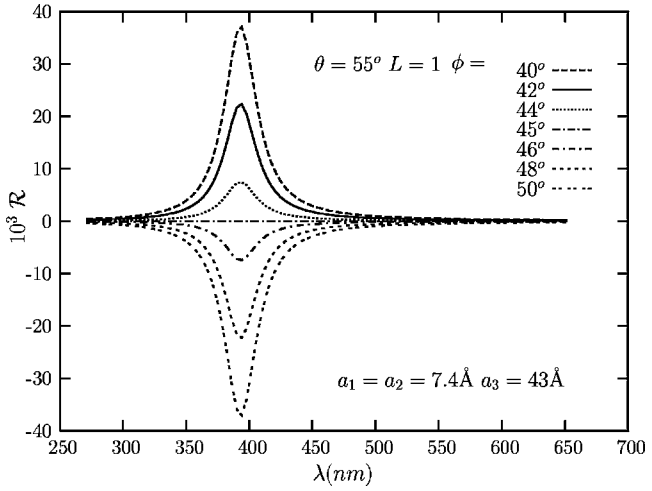

FIG. 4. $\mathcal{R}$ vs λ for a square 2D lattice with $L=1$ and $\theta=55°$, and for several values of ϕ.

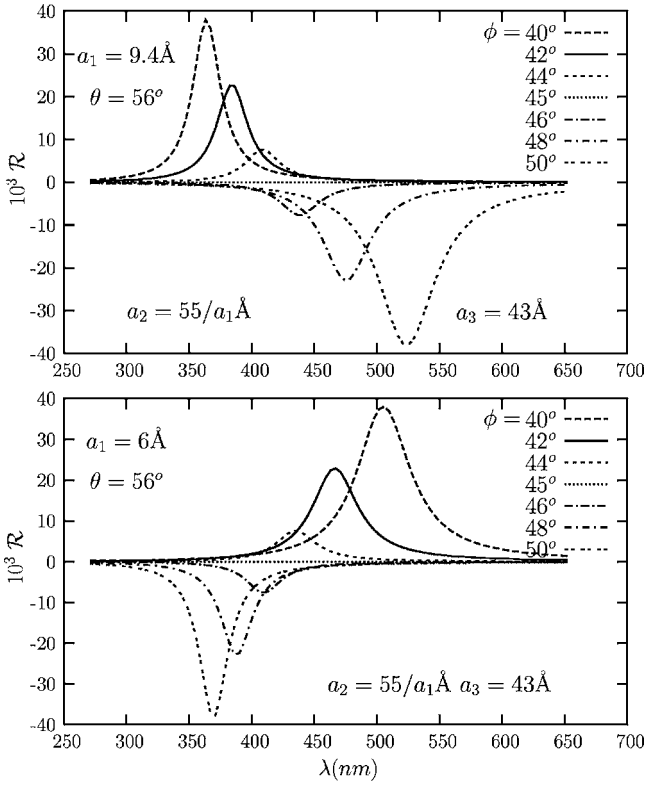

FIG. 5. $\mathcal{R}$ vs λ for a rectangular 2D lattice with $L=1$ and $\theta = 56°$, for several values of ϕ, taking $x \| \boldsymbol{a}_1$. Upper (lower) panel $a_1 > a_2$ ($a_1 < a_2$).

shifted) as ϕ increases. In the case of the centered rectangular and oblique lattices the behavior of $\mathcal{R}$ with ϕ depends on the value of γ (Fig. 2). If γ is equal to or around 45° the behavior is similar to that of a square (and hexagonal) lattice, because for this value of γ, $T_{xx} \approx T_{yy}$ and the ϕ-dependence in $\mathcal{D}$ is negligible. However, if γ is not around 45° we have $T_{xx} \neq T_{yy}$, and the ϕ-dependence in $\mathcal{D}$ is strong, just as for the rectangular lattice. The fact that $T_{xx} \neq T_{yy}$ can be seen as an intrinsic surface anisotropy, which is responsible for the shift in frequency of the peak-like structure shown in Fig. 5.

The behavior of Figs. 3–5, is actually found in all the 2D lattices and is independent of the value of L. Therefore, from these figures, we learn that for a system in which the polarizable entities of all the layers have the same values of θ and ϕ, the spectrum always presents a peak-like structure and that the magnitude and resonant frequency are functions of the angles θ and ϕ. However, the experimental results of Ref. 4 show that $\mathcal{R}$, goes from a peak-like to a derivative-like line shape as the number of deposited layers increases. We find that our model reproduces such results, if we allow for different values of θ and ϕ for each plane. Indeed, in Fig. 6 we show, for the square lattice, $\mathcal{R}$ for $L=2$, along with the imaginary part of the dipole polarization components $\mathrm{Im}(p_x(\ell))$ and $\mathrm{Im}(p_y(\ell))$ for the two planes. For $\ell=1$ $\phi_1 = 42°$ and $\theta_1 = 55°$ and for $\ell=2$ $\phi_2 = 48°$, and we take two different values of $\theta_2 = 56°$ and 54°. First of all, we see that $\mathcal{R}$ of both configurations has a derivative-like lineshape. For $\theta_1 < \theta_2$ ($\theta_1 > \theta_2$), $\mathcal{R}$ is positive (negative) for short wave-

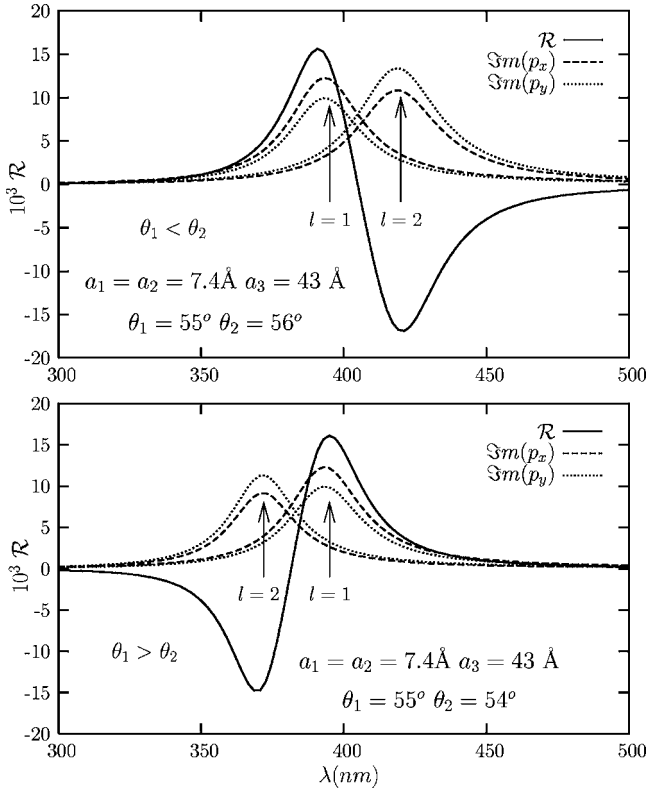

FIG. 6. $\mathcal{R}$, Im(p_x) and Im(p_y) vs λ for a square 2D lattice with $L=2$. $\phi_1=42°$, $\theta_1=55°$, $\phi_2=48°$, and $\theta_2=56°$ (upper panel) or $\theta_2=54°$ (lower panel). Notice that Im($\boldsymbol{p}$)($\ell=1$) is the same in both panels but that Im($\boldsymbol{p}$)($\ell=2$) moves from the right (upper panel) to the left (lower panel).

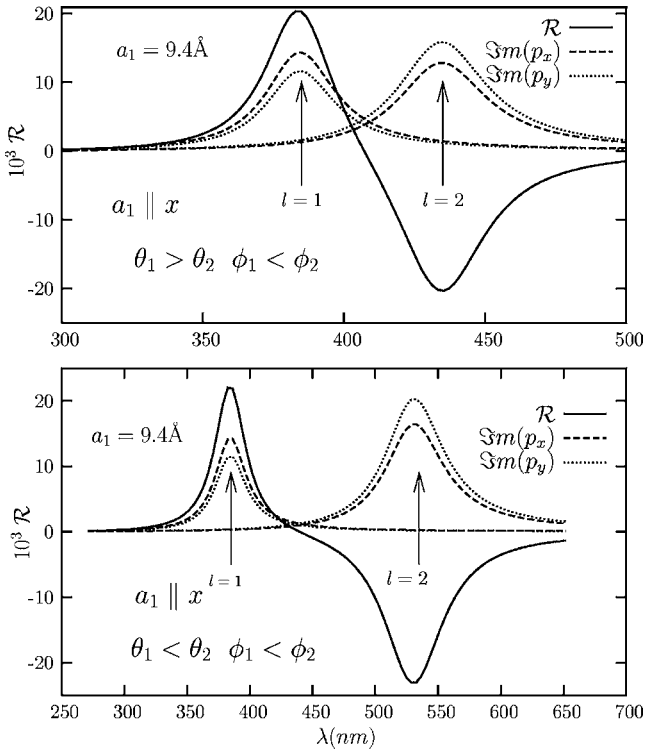

FIG. 7. $\mathcal{R}$, Im(p_x), and Im(p)$_y$ vs λ for a rectangular 2D lattice with $L=2$, $\theta_1=56° > \theta_2=55°$ (top panel) and $\theta_1=56° < \theta_2=57°$ (bottom panel). Notice the different range of λ for both panels.

lengths and negative (positive) for large wavelengths. This change from positive to negative or vice versa in $\mathcal{R}$, is understood in terms of the induce dipole acquired by each plane. As we explained above, both the resonant frequency and magnitude of the polarization are in general a function of the angles θ and ϕ, but for the square or hexagonal lattice the resonant frequency is function only of θ, and ϕ only controls the magnitude of $\boldsymbol{p}$. In Fig. 6 we see that the resonant frequency of the polarization of each plane is at different frequency due to the fact that each has a different angle θ, and has different magnitude in view of the different values of ϕ. Thus, when we subtract Im[$p_x(\ell)$] from Im[$p_y(\ell)$], we get a positive or a negative peak in $\mathcal{R}$, which alternates as a the wavelength is changed, and therefore gives the derivative-like line shape. For instance, for $\theta_1 < \theta_2$, the first plane has Im(p_x) > Im(p_y) and in the second plane the opposite occurs: Im(p_y) > Im(p_x). Therefore, in the first plane Im(p_x) − Im(p_y) will be positive and in the second plane Im(p_x) − Im(p_y) will be negative. Thus when we evaluate Eq. (11), we obtain that the RAS line shape has two peaks of different sign forming a derivative like spectrum. Notice that the position for the resonance of the polarization for the second plane is blueshifted as θ_2 is decreased (lower panel), whereas the polarization of the first plane remains fixed by the obvious reason that its parameters are fixed. Therefore, the negative peak in $\mathcal{R}$ comes from the second plane, and its negative in view of $\phi_2 > 45°$. If both ϕ_1 and ϕ_2 are smaller (larger) than 45°, $\mathcal{R}$ would show two positive (negative) peaks. By the same token for $\theta_1 > \theta_2$, if we take $\phi_1 > 45° > \phi_2$, we would get $\mathcal{R}$ going from positive to negative values as λ is increased, but the positive (negative) peak will come from the second (first) plane.

In Fig. 7, we show $\mathcal{R}$ and Im($\boldsymbol{p}$) for a rectangular lattice with $L=2$, for $a_1 > a_2$ and for both $\theta_1 > \theta_2$ and $\theta_1 < \theta_2$. For $\theta_1 > \theta_2$ we see that since Im(p)$_x(\ell=1)$ > Im(p)$_y(\ell=1)$ and Im(p)$_x(\ell=2)$ < Im(p)$_y(\ell=2)$, $\mathcal{R}$ goes, as λ increases, from a positive peak to a negative peak, in a derivative-like fashion. In contrast, when $\theta_1 < \theta_2$ we see that the resonant peaks of the polarization in the first and second planes are separated in λ (notice the different range of λ in Fig. 7), such that there is almost no overlap of the off-resonant part of the polarization, giving a lineshape that resembles more two isolated resonances, one positive and one negative, than a derivative-like lineshape. To complement Fig. 7, in Fig. 8, we show $\mathcal{R}$ for values of a_1 smaller and larger than a_2, passing through the square lattice, and always using $a_2=A/a_1$, and taking $a_1 \parallel x$. We see that the peaks in $\mathcal{R}$ change from positive to negative for increasing λ, as the lattice goes from an oblate, $a_1 > a_2$, to a prolate rectangle, $a_1 < a_2$, where we include the square lattice, $a_1=a_2$.

From Figs. 6–8, and equivalent behavior found for the other three lattices, we see that for a system with more than one molecular layer, allowing the upper layers to reorient with respect to the underlying ones, $\mathcal{R}$ acquires a derivative-like line shape. This behavior is directly related to the mag-

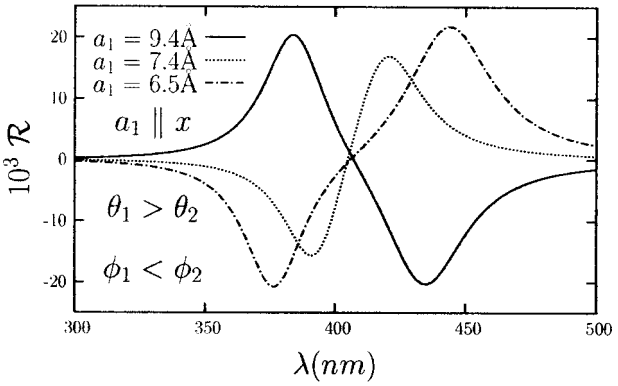

FIG. 8. $\mathcal{R}$ vs λ for an oblate ($a_1 > a_2$, solid line), square ($a_1 = a_2$, dotted line), and prolate ($a_1 < a_2$, dashed-dotted line), lattice, with $a_2 = 55/a_1$ Å, $a_3 = 43$ Å, $L = 2$, $\phi_1 = 42° < \phi_2 = 48°$, $\theta_1 = 56° > \theta_2 = 55°$, and $a_1 \| x$.

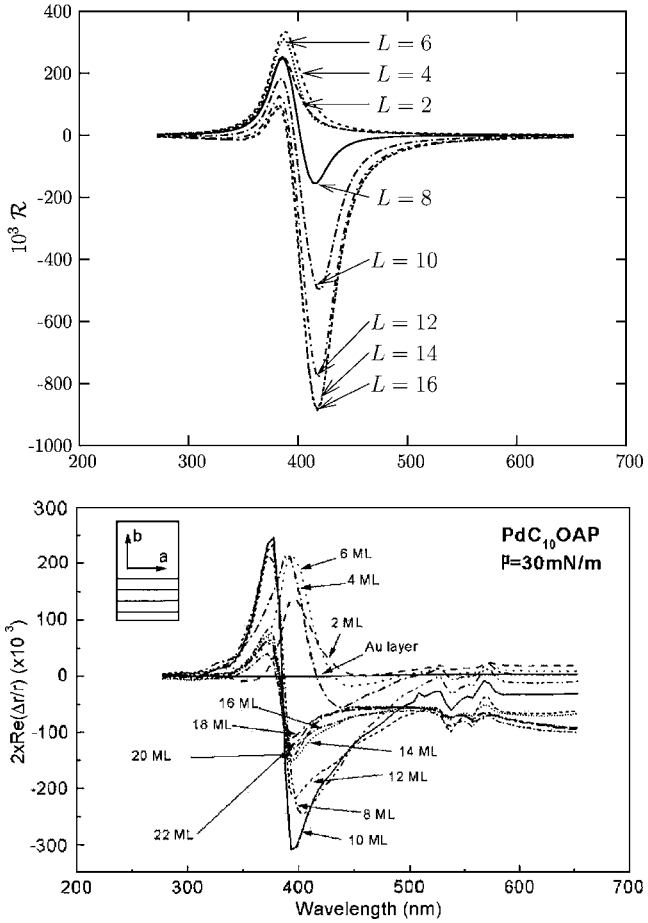

FIG. 9. Upper panel: $\mathcal{R}$ vs λ for a rectangular 2D lattice and several values of L. $\phi = 42$, $\theta = 56°$, $a_1 = 9.4$ Å, $a_2 = 55/a_1$ Å, $a_3 = 43$ Å, $\Delta\theta = -0.2$, and $\Delta\phi = 0.8$. In this case the largest side of the rectangle is parallel to the x axis. Lower panel: experimental results take from Ref. 4. For an explanation of the y-axis notation used in lower panel (see Appendix A).

nitude of the induced dipole along the two mutually perpendicular surface directions x and y. We find that for the square, hexagonal, and prolate rectangular, prolate centered rectangular, and prolate oblique lattices, tilting the dipoles of the upper layers towards (away) the surface normal, produces a derivative-like line shape that goes from negative (positive) to positive (negative) values of $\mathcal{R}$ as λ is increased. The opposite behavior is found for the oblate rectangular, oblate centered rectangular, and oblate oblique lattices, in which for dipoles that get closer to (farther from) the surface normal in the upper layers, the derivative-like spectrum goes from positive (negative) to negative (positive) values of $\mathcal{R}$ as λ is increased.

IV. COMPARISON WITH EXPERIMENT

The previous figures show a comprehensive overview of the dependence of $\mathcal{R}$ on the different parameters that control the signal. For a given 2D Bravais lattice, the orientation of the dipoles in each plane, and the number of planes, basically determine the spectra. Now, we proceed to compare with experimental results. In a RAS experiment, one has to choose a fixed direction in the sample, and from this specify x and y. For instance, in crystalline surfaces, one of the surface crystal axis is used as the x direction, which fixes y and the subsequent sign of $\mathcal{R}$. In our previous examples, the x axis is always specified along a_1; however, it should be clear that if one chooses y to be along this direction, the sign of $\mathcal{R}$ would be reversed, and thus one should be careful and aware that when comparing with experiment, there is always the possibility of not using the same coordinate system. The experiments of Ref. 4 chose their coordinate system along the directions of the sample holder and not necessarily along any of the possible *intrinsic* directions of the porphyrin array. In addition, there is not direct evidence of what the actual array of porphyrins is like, so that we have to make some plausible assumption. As the layers of porphyrin are deposited, we could think that the interaction of the porphyrin's π orbitals with the substrate will be screened by the underlying layers, thus producing top layers of porphyrins which will try to align its dipole moment along the substrate normal.[4] The experimental results of Ref. 4 give a RAS signal with single positive peak (near Soret band energy of an isolated porphyrin), when the sample has less than eight layers, but as more porphyrin layers are deposited, the RAS develops into a derivative-like signal which goes from positive to negative values of $\mathcal{R}$ as the wavelength is increased (see Fig. 9). As we saw in Sec. III, we not only need a varying θ but also a changing ϕ in order to be able to produce the RAS signals with derivative-like line shapes. Recall that both θ and ϕ control the position and relative strength of the resonance in $\mathrm{Im}(p_x)$ and $\mathrm{Im}(p_y)$ of Eq. (12), that in turn control the line shape of $\mathcal{R}$.

Regardless of the chosen axes a positive $\mathcal{R}$ for low layer coverage, means that $\mathrm{Im}(p_x) > \mathrm{Im}(p_y)$, for which $\phi < 45°$. Going back to Fig. 6 for the square lattice, we see that the positive peak in $\mathcal{R}$ always comes from the polarization of the first plane ($\ell = 1$) and for $\theta_1 < \theta_2$ ($\theta_1 > \theta_2$) the second plane ($\ell = 2$) has a negative peak at higher (lower) λ, thus giving

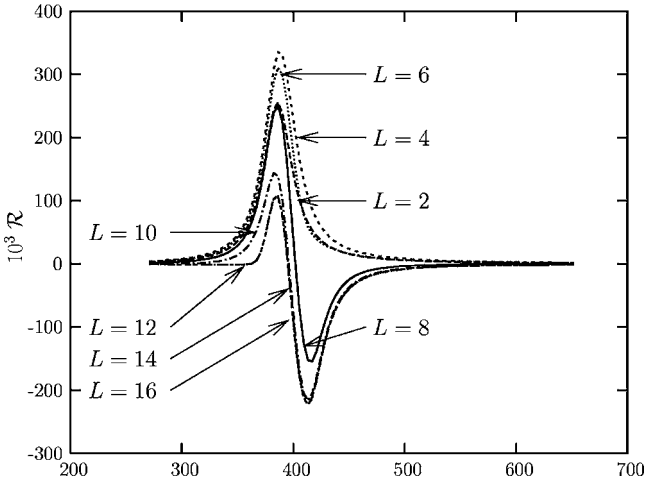

FIG. 10. Same as upper panel of Fig. 9, but $\phi=45°$ or $\theta=0°$ after $L=10$. See text for details.

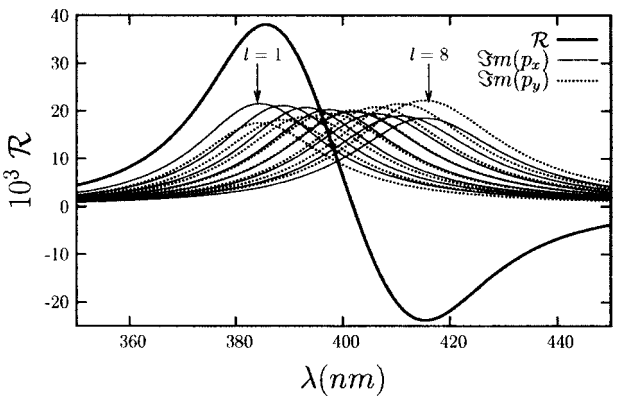

FIG. 11. $\mathcal{R}$ of Fig. 9 for $L=8$, along with the $\mathrm{Im}[p_x(\ell)]$ and $\mathrm{Im}[p_y(\ell)]$.

the derivative-like behavior, however the case for which $\mathcal{R}$ goes from positive to negative, corresponds to the top layer having a larger polar angle, contrary to the argument given above for the screening of the interaction by the lower layer. Now, for the rectangular lattice (Fig. 7), we see that for $\theta_1 > \theta_2$ if x is along the larger side of the oblate rectangle, the positive (negative) peak in $\mathcal{R}$ corresponds to the resonance of the polarization in the first (second) layer, giving a line shape in agreement with experiment. Notice that even if we interchange a_1 and a_2 in the square lattice, thus changing $\mathcal{R}$ into $-\mathcal{R}$, although we get the correct lineshape when $\theta_1 > \theta_2$, it would be wrongly identified, because the negative peak in $\mathcal{R}$ corresponds to the first layer, and we assumed, in agreement with the experiment, that the first layer gives a positive peak.[13]

Thus, for the experimental results of Ref. 4, our model implies that the porphyrins 2D unit cell could be an oblate lattice, in any of its three flavors, a simple rectangle, a centered rectangle, or an oblique rectangle, where the experimental x axis is along the larger side of the unit cell. Based on this assumption, we do a more detailed analysis and progressively change θ and ϕ as we increase L. In Fig. 9, we show $\mathcal{R}$ for the rectangular lattice of Fig. 7 for different values of L. For each corresponding growing change in L we decrease θ by 0.2° and increase ϕ by 0.8°, starting at $\theta=56°$ and $\phi=42°$ for $L=1$. Indeed, as L is increased the spectra goes from peak-like to derivative-like, and $\mathcal{R}$ goes from positive to negative values as λ is increased, in qualitative agreement with the experimental results also shown in Fig. 9.

We see in the experimental results that above 10 monolayers, the amplitude of the signal diminishes at all photon energies, rapidly converging to a limit value which remains steady up to the maximum thickness of 22 monolayers. The general trend of this behavior could be qualitatively reproduced by the model, if after some given plane, we take $\phi=45°$ or $\theta=0°$, for the remaining of the top planes, since for either case the signal of these planes will be zero, and the total RAS will then be constant. For instance, in Fig. 10 we have taken for $L=10$ an smaller value of ϕ, such that $\phi(L=8) > \phi(L=10) > 45°$, and after the tenth plane we fix $\phi(L>10)=45°$ and/or take $\theta=0°$. Now, the overall signal is more similar to the experiment. However, if these top layers are randomly disordered, one would expect equal projections of the induced dipoles along x and along y, giving also $\mathcal{R}=0$ for these layers, and disorder would explain the saturation of the signal. Our model could be extended for disordered layers in order to study the subsequent changes in the RAS signal, and thus give further insight into the morphological behavior of the possibly disordered top most layers, but this is out of the scope of the present article.

Finally, we mention that since the interplane local field interaction of a planar array, decays exponentially with z,[9] it follows that Eq. (12) is a good approximation for the total induced polarization of any given plane. Thus, the interpretation that we have given of the RAS spectra so far can be easily extended to any number of layers. As an example, we decompose $\mathcal{R}$ of Fig. 9 for $L=8$ into $\mathrm{Im}[p_x(\ell)]$ and $\mathrm{Im}[p_y(\ell)]$, as shown in Fig. 11. The resonances of $\boldsymbol{p}(\ell)$ readily allow us to interpret each plane's contribution towards $\mathcal{R}$, and the same analysis could be carried out for any value of L. We have also checked that changes of up to 10% in the interplane separation d, and the distance of the first layer to the substrate $d/2$, which up to now we fixed at $d=43$ Å, leave the results of Fig. 9 or Fig. 10 almost unchanged. The exponentially decaying interaction along z, also implies a negligible image contribution, which gives a lack of sensitivity to the substrate. Therefore, changing the substrate from a metal to a dielectric, by choosing the appropriate $\epsilon_2(\omega)$ in Eq. (9), has a negligible effect in the spectra. Thus, our model would apply to the films of Ref. 3, grown by the Langmuir-Blodgett technique on a quartz substrate.

All things considered, we readily see that the combined tilting and twisting of the dipoles in the different layers changes their polarization, through the local field effect, in such a way that the experimental signal can be accounted for in simple physical terms.

V. CONCLUSIONS

We have presented a theoretical study for the reflectance anisotropy spectroscopy (RAS), of molecular layers grown onto an isotropic substrate. The excitation of each molecule is modeled by an effective harmonic oscillator dipole moment that responds to local electric field. This local field includes the external electric field and the field induced by all the molecules of the system, avoiding self-interaction. We have obtained the RAS signal through the total polarization, and have shown that it depends on the structural parameters of the layers. In particular, we find a strong dependence on the polar and azimuthal angles, which describe the orientation of the dipole in any given layer, and the 2D Bravais lattice, that describes the ordering of the dipoles. As the tilting and twisting of the dipoles is varied for every molecular layer, we have shown that the spectra changes from a peak-like to derivative-like line shape. We have compared our theoretical predictions with experimental results on samples grown by the Langmuir-Schaefer technique on top of an isotropic gold substrate, and find that an oblate rectangular unit cell with an appropriate orientation of every layer qualitatively reproduces the measured RAS. The model supports the idea that at low coverage the molecules tend to be more inclined relative to the substrate, due to stronger interaction with it, but as the number of layers is increased the substrate influence decreases as it is screened by the underlying layers, and the molecules tend to straighten up. The model shows that the behavior of the system is ultimately driven by the local field among the molecules, and that their geometrical reordering, from layer to layer, as the sample is grown, qualitatively reproduces the experimental trend.

We expect our model to work equally well with any other molecule for which the long wavelength approximation holds, in particular molecules of the same size or smaller than the porphyrins of the experimental results shown here. If we would like to go beyond the harmonic point dipole approximation, a model like the one discussed in Ref. 7, that deals with elongated molecules, could be a good starting point to treat the porphyrins with a subtler microscopic model.

In conclusion, with the polarizable dipole model, we are able to explain qualitatively the optical RAS behavior of the growth process, and in principle determine parameters such as the tilt and twist angle and the 2D arrangement of the molecules of this very fascinating films.

ACKNOWLEDGMENTS

We acknowledge partial support from CONACyT-México (Grant No. 36033-E) and CONCYTEG-México (Grant Nos. 03-04-K118-039 anexo 5 and 04-04-K117-011 anexo 4).

APPENDIX A: RELATION BETWEEN THEORETICAL AND MEASURED RESULTS

In this appendix, we derive the relationship between $\mathcal{R}$ of Eq. (11) and $\Delta r/r$ of the experimental results of Ref. 4. The RAS experiment measures a normalized difference $\Delta r/r$ in the reflection coefficients, defined as

$$\frac{\Delta r}{r} = \frac{r_x - r_y}{(r_x + r_y)/2}, \tag{A1}$$

where r_x and r_y are complex reflection coefficients, for light polarized along x and y, respectively, with $\Delta r = r_x - r_y$, their difference and $r = (r_x + r_y)/2$, their average. $\Delta r/r$ is a complex quantity, whose real and imaginary parts exhibit different modulation frequencies which allow their measurement, one at a time, with a lock-in amplifier.[4] We can express $\Delta r/r$ in terms of reflectivity coefficients $R_i = r_i r_i^*$ (with $i = x, y$) and $R \equiv r r^*$ (the average reflectance), as follows:

$$\frac{\Delta r}{r} = \frac{(r_x - r_y) r^*}{r r^*} = \frac{(r_x r_x^* - r_y r_y^* + r_x r_y^* - r_y r_x^*)}{2 r r^*}$$
$$= \frac{R_x - R_y + r_x r_y^* - r_y r_x^*}{2R}, \tag{A2}$$

where the real part is

$$\mathrm{Re}\left(\frac{\Delta r}{r}\right) = \frac{R_x - R_y}{2R}. \tag{A3}$$

Our $\mathcal{R}$, of Eq. (11), was calculated through the following definition:[10]

$$\mathcal{R} = \frac{R_x - R_y}{R}, \tag{A4}$$

that in view of Eq. (A3), gives

$$\mathcal{R} = 2\,\mathrm{Re}\left(\frac{\Delta r}{r}\right). \tag{A5}$$

In conclusion, the calculated reflectance $\mathcal{R}$ is twice the measured RAS data.

[1] For a review see the articles in *Optics of Surfaces and Interfaces (OSI-2003)* [Phys. Status Solidi C 0, Num. 8 (2003); *WE-Heraeus-Seminar Optical Spectroscopy at Interfaces (OSI-2001)*, Phys. Status Solidi A 188, Num. 4 (2001).

[2] J. F. McGilp, Prog. Surf. Sci. **49**, 1 (1995).

[3] C. Goletti, R. Paolesse, C. Di Natale, L. G. Bussetti, P. Chiaradia, A. Froiio, L. Valli, and A. D'Amico, Surf. Sci. **501**, 31 (2001).

[4] C. Goletti, R. Paolesse, E. Dalcanale, T. Berzina, C. Di Natale, G. Bussetti, P. Chiaradia, A. Froiio, L. Cristofolini, M. Costa, and A. D'Amico, Langmuir **18**, 6881 (2002).

[5] B. G. Frederick, L. R. Power, R. J. Cole, C. C. Perry, Q. Chen, S. Haq, Th. Bertrams, N. V. Richardson, and P. Weightman, Phys. Rev. Lett. **80**, 4470 (1998).

[6] C. Castillo, R. A. Vázquez-Nava, and B. S. Mendoza, Phys. Status Solidi **0**, 2971 (2003).

[7] R. W. Munn and M. M. Shabat, J. Chem. Phys. **99**, 10052 (1993);

99, 10059 (1993).

[8] N. Arzate, B. S. Mendoza, and R. A. Vázquez-Nava, J. Phys.: Condens. Matter **16**, S4259 (2004).

[9] F. W. de Wette and G. E. Schacher, Phys. Rev. **137**, A78 (1965).

[10] W. L. Mochán and R. G. Barrera, Phys. Rev. Lett. **55**, 1192 (1985).

[11] From Eq. (12), we can scale $p_o=\delta(e^2f_0/m\omega_0^2)E$, with E the strength of the electric field, thus leaving δ to scale $\mathcal{R}$. We used $\delta=0.15$ to get the theoretical spectra of Fig. 9, and kept the same value throughout the article.

[12] J. H. Weaver, C. Krafka, D. W. Lynch, and E. E. Koch, *Physics Data Series* (Fachsinformationzentrum-Energy, Physik, Mathematik, Karlsruhe, 1981).

[13] For this reason, the square lattice in Ref. 6 was wrongly assigned.